UNIVERSITY OF BIRMINGHAM

Ex-situ experimental benchmarking of solid oxide fuel cell metal interconnects

Bianco, Manuel; Tallgren, Johan; Hong, Jong-Eun; Yang, Shicai; Himanen, Olli; Mikkola, Jyrki; Van Herle, Jan; Steinberger-Wilckens, Robert

[Link to publication on Research at Birmingham portal](#)

Ex-situ experimental benchmarking of solid oxide fuel cell metal interconnects

Manuel Bianco [a,*], Johan Tallgren [b], Jong-Eun Hong [c], Shicai Yang [d], Olli Himanen [b], Jyrki Mikkola [b], Jan Van herle [a], Robert Steinberger-Wilckens [e]

[a] *Group of Energy Materials, Inst. Mech. Eng., EPFL Valais, CH-1951, Sion, Switzerland*
[b] *VTT Technical Research Centre of Finland Ltd, Fuel Cell Solutions, P.O. Box 1000, FI-02044, Espoo, Finland*
[c] *Fuel Cell Laboratory–Korea Institute of Energy Research, 152 Gajeong-ro, Yuseong-gu, Daejeon, 34129, Republic of Korea*
[d] *Teer Coatings Ltd., West Stone House, West Stone, Berry Hill Industrial Estate, Droitwich, WR9 9AS, UK*
[e] *Centre for Fuel Cell and Hydrogen Research–School of Chemical Engineering, University of Birmingham, Edgbaston, Birmingham, B15 2TT, UK*

HIGHLIGHTS

- More than 60 combinations of material solutions for SOFC interconnects are tested.
- Chromium retention and area specific resistance of these solutions are measured.
- Coating deposition technique is the key for an interconnect of good performance.
- Cheaper commercial stainless steel (K41) can compete with SOFC-specific steels.
- Steel nitriding improves chromium retention when coatings are porous.

ARTICLE INFO

ABSTRACT

Solid oxide fuel cells (SOFCs) can convert hydrocarbon fuels, such as methane, into heat and electricity with a high conversion efficiency. The fuel flexibility of the SOFC derives from the high operating temperature (600-900 °C). Such a high temperature stresses the materials used in the SOFC stacks, notably the metals constituting the interconnect (IC). Research centres developed in last twenty years specific alloys and coatings compositions. This led to a vast literature production of solutions to mitigate the degradation of the metals used in SOFC stacks. Unfortunately, the testing method and conditions change from one laboratory to another making the comparison of the results often impossible. This article compares systematically more than sixty different solutions to limit the degradation in the IC. The samples differed for the steel composition, the coating deposition technique, and the coating composition. A modified 4-probe technique and SEM/EDS post-test characterization measure the area specific resistance and chromium retention of the samples. Testing results indicate that i) deposition technique is the most relevant parameter, ii) in presence of coatings, the performances are independent of the type of ferritic stainless steel substrate iii) nitriding helps to limit the outward chromium diffusion in case of porous coatings.

1. Introduction

A solid oxide fuel cell (SOFC) is an electrochemical device that converts fuels such as hydrogen or methane to heat and electricity at very high efficiencies. The operating temperatures of 600–900 °C require high temperature resistant materials, typically ceramics. The cathode catalyses an oxygen reduction reaction that supplies oxygen ions. These pass through the electrolyte, oxidising the fuel on the anode side, and thus producing electrons driving the electric current supplied by the SOFC. Commercially available devices have proven that SOFCs can reach system net electrical efficiencies of over 60%. In combined heat and power mode (CHP) they can reach 90% and more total efficiency [1,2]. The only emissions of an SOFC are water and carbon dioxide (if carbonaceous fuels are used), completely avoiding the generation of particulates, NO_x, or SO_2 in the exhaust, unlike typical fossil fuel power plant emissions. SOFCs supply a solution to

transitioning from the current natural gas grids to a carbon- and emission-free electricity and heat supply, as long as the fuel cell fuels are sourced from renewable sources [3]. This allows a smooth and seamless progression from a fossil fuel, carbon emitting, to a zero net carbon gas supply, avoiding the costly conversion of existing gas grids to hydrogen operation.

Single planar SOFC cells typically have sizes from 10×10 cm^2 to 25×25 cm^2 supplying 20 to over 500 W$_{el}$ per cell at typical operating conditions. To obtain a power output in the order of kW$_{el}$ and more, multiple cells have to be connected in series, to 'stacks'. Such stacks can be connected in parallel and series to form larger modules up to MW$_{el}$ size. In order to collect and conduct the electrical current, supply mechanical stability to the stack, and separate and direct gas flows, cells are connected by an 'interconnect' plate. In principle this interconnect could be made of ceramic or metallic materials, but owing to the superior electrical conductivity and ease of manufacturing, the common solution for interconnects today are ferritic stainless steels (FSS) [4].

Due to the specific operation conditions, i.e. high temperature, polarisation, exposure to oxidising and reducing atmospheres on opposite sides of the interconnect, these steels have to satisfy several requirements: impermeability to gas, low electrical contact resistance, creep resistance, resistance to corrosion, lack of reactivity with other stack materials, and finally, a coefficient of thermal expansion (CTE) that is compatible with the ceramic material of the SOFC cells [5].

To meet the needs of corrosion resistance, chromium containing steels, specifically stainless steels are chosen. A chromium content between 17 and 22 wt.% will serve to form a chromia layer that acts as passivation coating, slowing oxide scale growth. In order to meet the further requirements, especially that of CTE compatibility, ferritic stainless steels with very specific chemical compositions have been developed, such as Crofer 22 APU [6]. Albeit these beneficial properties, the use of the bare steel alone has proven to be unsatisfactory for interconnects since the reduction of chromium mobility was insufficient. For this reason, protective layers are commonly deposited on the surface of the metal interconnect (MIC). Protective layers further reduce oxide scale growth and substantially limit diffusion of chromium, including the formation of chromium hydroxide. This is volatile and leads to removal of chromium from the stack or at least migration from interconnect to cathode, negatively impacting on the latter's catalytic activity (cathode chromium poisoning) [7].

There is a considerable body of literature on protective coatings, with a wide choice of materials offered, differentiated by constituting elements and composition, deposition technique etc. [8]. For instance, spinel [9–16] and perovskite [17–22] coatings have frequently been used. Testing conditions differ between reports, making comparisons of results difficult. As an example, the electrical properties of Crofer 22 APU in three recent papers [14,23,24] were all measured with the 4-probe testing method, but the temperature, the cathode materials, the contacting materials, the current density, the testing time, and the compression force are never identical. The SCORED 2:0 project, funded within the Horizon 2020 EU framework through the FCH JU, has ventured to systematically analyse the interaction between coating materials, steel substrates, and coating techniques to find combinations that offer the best solution with respect to contact resistance, corrosion resistance, and reduction of chromium evaporation.

The benchmark was set as the Sanergy HT (SS HT) steel coated by physical-vapour-deposition (PVD) with a very thin Ce/Co protective coating and produced by Sandvik. This material shows excellent properties in terms of low area specific resistance (ASR) in the order of 5–10 mΩ*cm^2 and good chromium retention. The criteria of ASR and chromium retention are chosen to define the performances of the studied samples because of their contribution to cathode side degradation in a stack. A disadvantage in the application of the PVD deposited Ce/Co coating and SS HT is their cost.

This study aimed to find solutions that matched or even surpassed Cr retention and contact resistance performances of the SS HT Ce/Co

reference samples, thus offering more variety and versatility in manufacturing, and a potential for cost reduction. The samples presented in this study varied in the type of stainless steel substrate, coating composition, coating deposition technique, and the pre-treatment of the steel surface by nitriding prior to coating. This article presents and compares data obtained with *ex-situ* tests on more than 60 steel/coating combinations on small (1×1 cm^2) samples.

2. Materials and experiments

Table 1 describes the types of steel/coating combinations evaluated in this study.

The first column lists the deposition techniques used: wet powder spraying (WPS), atmospheric plasma spraying (APS), physical vapour deposition (PVD), and atomic layer deposition (ALD).

Coatings were produced by SOLIDpower S.p.a. (WPS 1), Turbocoating S.p.a. (APS), Teer Coatings Ltd (PVD), University of Birmingham (WPS 2), and VTT Technical Research Centre of Finland Ltd (ALD). The reference Sanergy HT coated with cerium and cobalt was purchased from AB Sandvik Materials Technology [25]. Details of the coating procedures are given further below.

Except for WPS, the deposition techniques produced dense coatings on the steel substrate surface: tens of μm thickness (50–60 μms) for APS, few to several μms (1–10 μms) for PVD, between 10 and 30 μms for WPS, depending on the supplier, and nanometric thin barrier layers for ALD. The coating composition columns list the different protective layer materials applied: $MnCo_2O_4$ (MCO), $MnCo_{1.8}Fe_{0.2}O_4$ (MCF), and $MnCo_{1.6}Fe_{0.2}Cu_{0.2}O_4$ (MCFC). A cerium/cobalt coating deposited via PVD is also present in the table. This sample represented the benchmark pre-coated Sanergy HT substrate. The selected MIC materials employed, and described in the steel column, are the ferritic stainless steels AISI441/K41, Crofer 22 H, and Sandvik Sanergy HT. The compositions of these steels are given in Table 2.

Three combinations were not included in the current study for a number of reasons (Table 1): APS-deposited MCFC (in batch 4), ALD-deposited MCF on nitrided steel (in batch 5), and WPS 2-deposited MCF on nitrided steel. MCFC powders were not compatible with the APS technology; after 4 batches ALD coatings did not produce results good enough to justify a 5th batch; and WPS 2 batch coating 5 could not be produced on time. In the first batch, Crofer22H samples are mostly missing (except for ALD coatings) due to a supply issue.

2.1. Sample preparation

Batches 2 and 5 had the same coating composition as batches 1 and 3, respectively, with the difference that the stainless steel substrates were nitrided before coating. Plasma nitriding was performed using a pulsed DC glow discharge plasma in a cylindrical vacuum chamber that applied a conventional 4-magnetron closed field configuration with a diameter of 550 mm and height of 600 mm. The substrate turntable had a diameter of 350 mm with single fold rotation. The total combined surface area of the biased rotation table was approx. 0.3 m^2. Argon or Argon mixed with other gases was introduced into the vacuum chamber and the gas flow was adjusted to maintain a pressure of 1.33 Pa throughout the process.

The process started with pure Ar plasma to clean the surface for about 20 min and then to introduce an Ar/N$_2$ plasma in a gas flow ratio of 1/3 and a pressure of 1.33 Pa. The turntable was biased by a pulsed plasma power generator (AE Pinnacle™ Plus) with the following parameters: power up to 6.0 kW (equal to 2.0 Wcm^{-2} or 3.3 mAcm^{-2} on the substrate), frequency up to 350 kHz, positive pulse width up to 1600 ns, implying a duty cycle of 44%, and negative bias potential as low as -600 V (adjustable). The depth of nitriding depended on time and power applied in the process.

ALD coatings were applied with a Picosun SUNALE R-200 reactor. Precursors used were Mn(thd)$_3$, Co(thd)$_3$ (abcr GmbH & Co), ferrocene

Table 1
Overview of sample combinations tested in this comparative study.

Coating Method	BATCH 1 Coating	BATCH 1 Steel	BATCH 2 Coating	BATCH 2 Steel	BATCH 3 Coating	BATCH 3 Steel	BATCH 4 Coating	BATCH 4 Steel	BATCH 5 Coating	BATCH 5 Steel
ALD	MCO	Crof 22 H / K41 / SS HT			MCF	Crof 22 H / K41 / SS HT	Ce + MCO	Crof 22 H / K41 / SS HT		
APS	MCO	K41 / SS HT	SAME COATING COMPOSITIONS AS BATCH 1 WITH NITRIDED SUBSTRATES		MCF	Crof 22 H / K41 / SS HT			SAME COATING COMPOSITIONS AS BATCH 3 WITH NITRIDED SUBSTRATES	
PVD	MCO	K41 / SS HT			MCF	Crof 22 H / K41 / SS HT	MCFC	Crof 22 H / K41 / SS HT		
WPS 1	MCO	K41 / SS HT			MCF	Crof 22 H / K41 / SS HT	MCFC	Crof 22 H / K41 / SS HT		
WPS 2	MCO	K41 / SS HT			MCF	Crof 22 H / K41 / SS HT	MCFC	Crof 22 H / K41 / SS HT		
PVD	CeCo	SS HT								

Table 2
Element composition of the steel substrates used (wt.%).

	Fe	Cr	C	Mn	Si	Al	Mo	Nb	Ti	W
K41/AISI 441 [26]	Bal.	18	0.012	0.3	0.35	–	–	0.45	0.17	–
Sanergy HT [27]	Bal.	21.2	0.04	0.3	0.12	0.017	0.96	0.71	0.09	–
Crofer 22H [27]	Bal.	20.0–24.0	0.0–0.03	0.0–0.80	0.1–0.60	0.0–0.10	–	0.2–1.0	0.02–0.20	1.0–3.0

FeCp$_2$ (Aldrich), Ce(thd)$_4$ (Volatec Ltd) and ozone O$_3$ (thd = 2,2,6,6-tetramethyl-3,5-heptanedionato and Cp = cyclopentadienyl). Prior to coating, the substrates were cleaned in an ultrasonic bath with ethanol, after which they were wiped with acetone. MnCo$_2$O$_4$ ALD-coatings were manufactured as one homogenous layer. MCF and Ce/Co coatings were deposited in two phases. For the MCF coating, a 100 nm thick (MnCo)$_3$O$_4$ layer was first deposited. Then, an approximately 10 nm thick layer of Fe$_2$O$_3$ was added on top. For the Ce/MnCo ALD-coating (batch 4), first an approximately 15 nm thick cerium oxide was deposited which was followed by a 130 nm thick (Mn,Co)$_3$O$_4$ coating.

For WPS 1 coatings, a conventional spray was applied with suspensions that were prepared by ball milling (with zirconia balls) from a mixture of binder, solvent, and commercial protective layer powders. The steel substrates of ASR samples were ground with SiC paper up to #1200 grit and then ultrasonically cleaned in acetone and ethanol respectively. The WPS 2 coating was carried out under the following conditions: 3 mm nozzle diameter, 2.0 bar spraying pressure, and 10 cm distance of nozzle to substrate. Sprayed samples were heat-treated in 4% H$_2$–Ar with 3% H$_2$O (100 ml/min) °C for 2 h and subsequently in air (100 ml/min) for 10 h at 800 °C.

Details on other deposition techniques are proprietary information of the fabrication partners.

2.2. Testing

A modification of the 4-probe technique was developed [28] to characterise the contact resistance and the Cr retention of each steel-/coating sample combination. A 0.2 mm thick steel sample 10*10 mm^2 lamella with a connection bracket coated with the desired protective layer was contacted to a symmetric L-shaped 0.5 mm thick Pd lamella screen printed on one side with a 20 ± 2 μm thick lanthanum strontium cobaltite (LSC).

These two coupons were then assembled with the coated sides facing each other, simulating an SOFC cathode–interconnect contact. Such couples were then piled on top of each other into a tower usually made of 10–12 samples. Voltage lead wires were welded to the protruding smaller leg of the L-shaped samples. Alternatively, a thin platinum wire was inserted through a hole drilled in the same leg and then tightened

into a knot. Current was supplied through gold or palladium wires, and set to give a current density of 0.4 Acm^{-2} through the samples.

The samples tower was compressed under 0.4 MPa in a clamping set-up, heated up to 700 °C (50 °C/h heating ramp) inside a Rohde TE 70 QT furnace and maintained for 1000 h in humidified compressed air atmosphere (3 vol.% H$_2$O). Air is humidified passing through a bubbler placed outside the furnace, at room temperature. The air flow, controlled with a Vögtlin V-100 rotameter, was set to 1 NL/min. An alternative description of the testing method can be found in Ref. [27]. The voltage between the Pd and the steel substrate is measured every 5 min (Agilent 34970a data acquisition device) during 1000 h of aging at 700 °C. The acquired signal noise was below 0.5 mΩ*cm^2 and the values used to build Fig. 1 come from the average of the 12 measurements taken in the 1000th hour of the ASR test. This experimental setup simulated the contact situation of cathode and interconnect, including the

- Compression = 40 N
- Contact area = 1 cm^2
- Current density = 0.4 Acm^{-2}
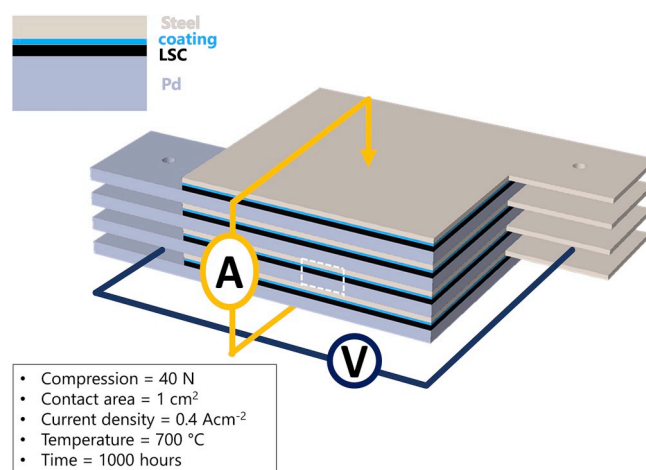- Temperature = 700 °C
- Time = 1000 hours

Fig. 1. Schematic representation (not to scale) of the modified 4-probe testing set-up for the area specific resistance measurement. On the top left a magnification of the area highlighted with white dotted lines and in the bottom left the testing conditions.

chromium migration by solid state diffusion. It did not capture the effect of chromium hydroxide formation and volatilisation. Nevertheless, basic information on this process was also captured in that the chromium hydroxide formation requires a diffusion of chromium through the oxide scale and protective layer.

In the case of perfect contact between the coating material and the perovskite conductive material, the oxide layer grown at the steel/coating interface is the main contributor to the ASR values. The electrical conductivity of spinels is, at least, two orders of magnitude higher than that of the scale [8].

After completion of the tests, the samples were extracted from the test furnace and, while maintaining a spring-like compression, embedded in epoxy resin (Sigma Aldrich Epoxy embedding kit). The embedded block was cut with a diamond saw and manually polished up to 1 μm grit with diamond paste. Cross sections were then analysed using scanning electron microscopy (SEM, FEI TENEO) and energy dispersive x-ray spectroscopy (EDS, Bruker), operating in the beam energy range of typically 15–30 kV. The chromium retention of the coating was assessed quantifying the amount of chromium that had diffused into the LSC layer cross section using EDS line-scan quantification. The values reported in Fig. 3 constitute the average over each line-scan. EDS accuracy and

lower detection limit were considered to be around 1 at.%.

3. Results and discussion

Figs. 2 and 3 give an overview of the results, correlating the sample notations of Table 1 with the experimental results. The chromium retention of the coatings and their ASR values taken after 1000 h of testing are plotted as functions of the steel type, the coating deposition technique, and the coating composition.

The area specific resistance and Cr retention performances of the coatings are grouped in two separated charts. Each of the two parameter is organised according to the coating deposition technique; i.e. in Figs. 2 and 3 there is one graph each for ALD, APS, PVD, WPS 1, and WPS 2.

The colour of the bars helps to identify the different coating composition and, if present, the nitriding process of the steel substrate: red indicates standard steels coated with MCO, blue indicates nitrided steels coated with MCO, black indicates standard steels coated with MCF, green indicates standard steels coated with MCFC, yellow indicates standard steels coated with Ce + MCO and finally purple indicates nitrided steels coated with MCF. The pattern inside the bar in turn indicates the type of the steel substrate: solid colour for AISI441/
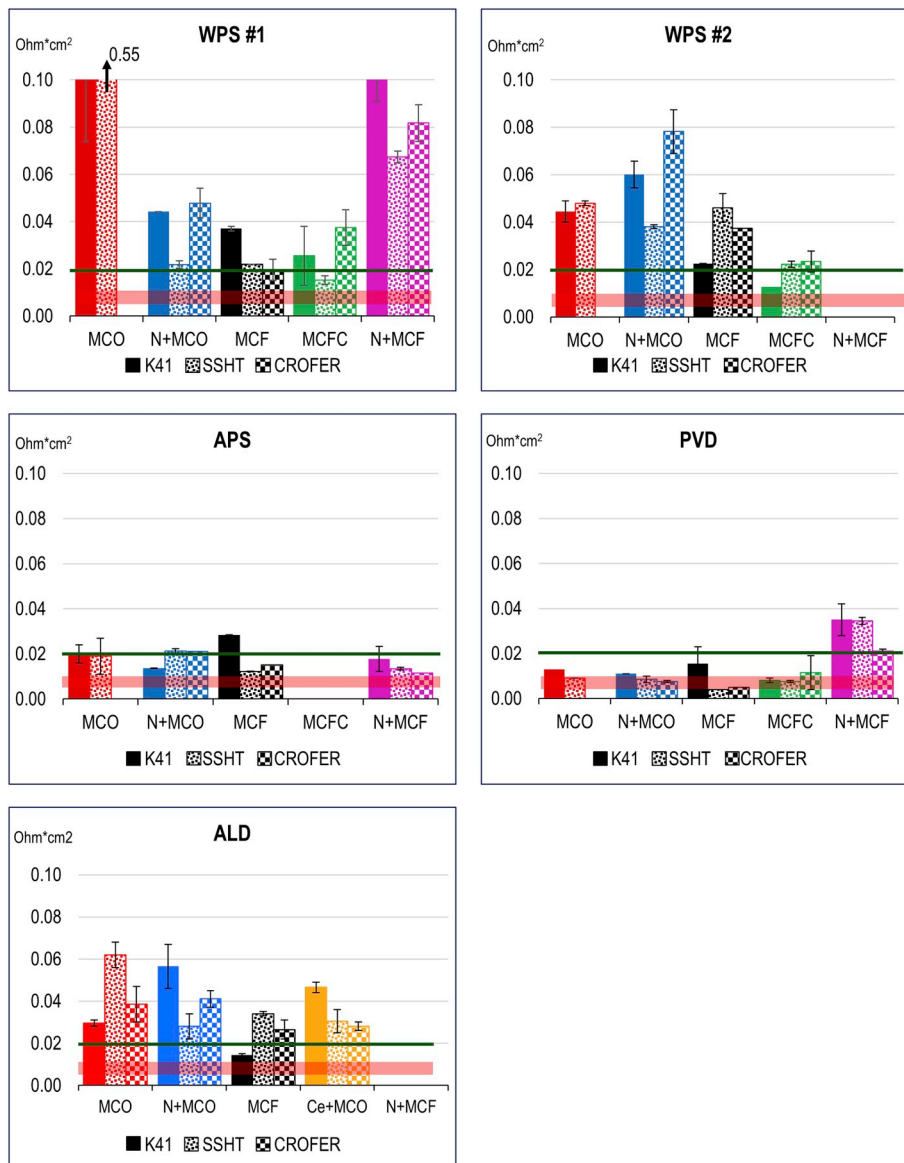
Fig. 2. ASR results of small, coated steel samples after 1000 h of testing at 700 °C. The bar charts show the area specific resistance value as a function of the coating composition and technique, and substrate processing. The error bars display the range between the minimum and maximum values, typically of two tested samples. The pink bar represents the performance range of Sandvik Sanergy HT Ce/Co, the green line indicates a threshold of 20 mΩ*cm.² (For interpretation of the references to colour in this figure legend, the reader is referred to the Web version of this article.)

Fig. 3. Cr retention properties of the ASR tested small coated steel samples. The green line at 1 at.% indicates the threshold of detection and the goal set here for an effective chromium retention. Above this limit the coating is considered not to succeed in reducing Cr diffusion. The values are calculated on the basis of the average of chromium found in the LSC coating contacting the interconnect samples. (For interpretation of the references to colour in this figure legend, the reader is referred to the Web version of this article.)

K41 substrate, checkered for Crofer 22 H substrate, and the dotting for Sandvik Sanergy HT substrate. The green line in both Figures represents the target to achieved so that the tested solution would be considered successful. For contact resistance this indicates an ASR value below 20 mΩ*cm² after 1000 h of testing. For the chromium retention properties, the target is set at 1 at.% Cr presence in the LSC, considered to be the minimum significant threshold for EDX detection. A bar above this threshold meant that the coating did not succeed in sufficiently reducing chromium diffusion. Finally, the pink transparent band represents the region of the performance obtained with the Sandvik Sanergy HT PVD pre-coated steel with Ce/Co coating adopted as the reference case.

3.1. Steel substrate

Figs. 2 and 3 show that no specific steel consistently delivered better results than the alternatives in terms of contact resistance and Cr retention. The influence of the deposition technique and the coating composition will be discussed later. According to these results and testing conditions, commercial ferritic stainless steels with a chromium content of 17–18 wt.% are an equivalent alternative to higher alloyed

steels, when coated. Though ferritic stainless steels such as Crofer 22 (H or APU) and SS HT have been designed specifically for use in SOFC interconnects, they do not sufficiently protect against chromium migration, if uncoated.

Specifically, high chromium content aims to grow a protective and stable Cr_2O_3 layer at high temperature on the steel surface. Further alloying elements are added to the alloy in order to improve specific properties of the steel. Manganese is added to lower the kinetics of oxide scale growth and electrical resistivity of the scale by forming a $(MnCr)_3O_4$ spinel on its surface. Niobium and/or tungsten are added to react with iron and chromium to segregate Laves phases at the grain boundaries. These precipitates increase the creep resistance of the material hindering dislocation motions [29]. Addition of reactive elements such as lanthanum improves the oxide adhesion on the steel substrate [30].

The production of these special types of steel, currently done at relatively small scale, contributes to their high cost. Crofer 22 APU (similar to Crofer 22 H in this study) is about one order of magnitude more expensive than AISI441/K41 [31]. Because the cost of interconnects accounts for 10%–30% of the total stack manufacturing cost

[31,32] using a cheaper, lower alloyed steel can be significant in improving SOFC market competitiveness.

On the other hand, this result must be taken with caution, as 1000 h is a short period compared to the desired operational time of the SOFC device. However, the interactions among the materials take place immediately after start of the exposure. Therefore, even if the corrosion process continues over the lifetime, at 1000 h basic interaction phenomena taking place at the interfaces are already visible. Among the different processes occurring at the MIC/cathode interface, most of the ohmic loss should stem from the thermally grown oxide scale at the steel/coating interface since this is a semiconducting material [33]. Ideally, given the definition of ASR (Ω*cm^2), it would be roughly sufficient to divide the ASR values by the average scale thickness in order to obtain the resistivity values (Ω*cm) of the scale. However, the resistivity values calculated with this method are not consistent. For example, the resistivity calculated for AISI441/K41 WPS 2 (MCO coating on nitrided substrates) and for batch 3 (Fe-doped MCO on standard substrates) differ by orders of magnitude. The reason for this lack of homogeneity might be: i) the different scale composition, ii) the scale morphology and irregularity, and iii) the real contact area not matching with the theoretical one.

The EDS analysis on the scale layer indicates that the standard corrosion products formed at the steel/coating interface are generally discontinuous SiO_2 and bulk Cr_2O_3. A spinel of chromium and manganese is also expected at the interface between the corrosion layer and the coating, but the Mn signal originating from the coating hinders the identification through EDS analysis. Considering the corrosion products, only the samples coated via APS yield thin oxide layers with regular thickness. In other samples, notably for PVD and WPS, an irregular inward corrosion is found (Fig. 4). These regions have complex oxide compositions: EDS analysis shows significant quantities of cobalt and iron, besides the expected chromium, manganese, and oxygen.

The oxide compounds containing these elements have differing stoichiometry and therefore different electrical conductivities. It follows that in these experiments it is not possible to calculate a consistent theoretical resistivity for the corrosion layer.

Regarding the influence of nitriding, comparing the results displayed in Figs. 2 and 3, the samples with the lowest contact resistances do not match those with the best Cr retention properties. Nitrided samples, in particular, present excellent Cr retention properties despite modest ASR

values. Among all the nitrided substrates coated with MCO or MCF, only ALD MCO coated Crofer 22 H show a potential Cr contamination risk (1 at.%).

In the steel samples used for ASR assessment, the EDS analysis indicated the precipitation of Cr_2N particles. The formation of Cr_2N and CrN is a known reaction taking place in the nitrided steel substrate, for instance used for low temperature, polymer electrolyte fuel cell (PEFC) applications [34]. The migration of chromium towards the steel surfaces was mitigated by the reaction with the nitrogen, which has a positive effect in the case of porous coatings.

3.2. Coating

$MnCo_2O_4$ spinel was the base reference coating material chosen for this study. This compound has been applied in SOFC for almost 20 years and proved to guarantee good electrical conductivity and Cr retention [35]. A partial replacement of cobalt was attempted during the project using a 1:1 Co:Mn stoichiometry in place of the usual 2:1. However, difficulties in producing powders with this composition hampered further developments [36]. As an alternative to a decrease in cobalt content, MCO was doped with Fe or Fe + Cu in batches 3 and 4. The addition of these elements was expected to be beneficial to increase the spinel electrical conductivity [37] and decreasing the sintering temperature. Detailed information on results obtained with Fe-doped MCO spinel-coated samples have been published separately [27].

Among absolute ASR performances after 1000 h of testing, the lowest average value was registered for Fe-doped MCO deposited by PVD on SS HT and Crofer 22 H: 5 mΩ*cm^2 (Figs. 2 and 3). APS and PVD deposition, due to the high density of these coatings, guaranteed repeatability of results independently of the coating composition, with ca. 90% of the average ASR values being lower than 20 mΩ*cm^2. Alternatively, according to a more conservative estimation, the 80% of the ASR higher values are below 25 mΩ*cm^2. Conforming to the definition of chromium retention given in the materials and experiments section, no Cr contamination is detected in the LSC layers when using APS or PVD.

Doping of MCO with Fe and Cu demonstrated a significant decrease of the ASR for wet powder sprayed coatings with respect to the original MCO coated samples. Only the MCF coated SSHT substrate in WPS 2 has in fact an ASR value similar to that of MCO. Notably, the K41 substrate samples significantly improved for both WPS coatings. This
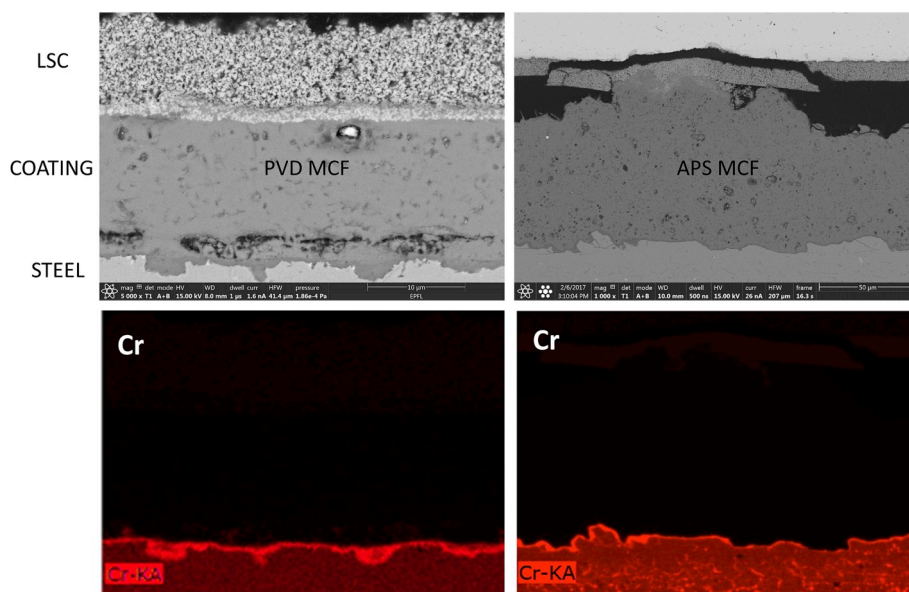

Fig. 4. Examples of cross sections taken from ASR samples containing PVD and APS deposited coatings after 1000 h at 700 °C, specifically MCF. EDS element mapping displays that for the PVD coated sample, the corrosion layer profile is inhomogeneous.

improvement was obtained independent of the type of steel substrate. Based on SEM observations, this improvement in performance related to the densification of the protective coating (Fig. 5). A denser coating hampers the chromium evaporation and the subsequent $SrCrO_4$ formation at the coating/LSC interface. Strontium chromate is a phase with low electrical conductivity and its absence improved the ASR performance. It is again confirmed that densification of the coatings is a key aspect.

Another example stems from the ASR results of MCO coatings, batch 1. The samples with coatings deposited by PVD were measured with values in the 10–20 mΩ*cm^2 range, while the WPS -deposited ones showed values between 40 and 500 mΩ*cm^2.

A dense coating is a necessary condition, but it is not sufficient in its own. ALD-deposited coatings were non-porous, but post-test characterisation on ASR test samples revealed their failure in protecting the steel from Fe-breakaway corrosion (Fig. 6). Presence of Cr in the LSC layer demonstrated failure in chromium retention.

Fig. 6 shows ALD-deposited MCO coatings, on standard SS HT substrate (top in Fig. 6) and on nitrided SS HT (bottom in Fig. 6). The difference in image quality is due to the use of FIB ion milling for the cross section observation of the nitrided sample. In both cases, the coating failed to prevent iron outward migration. For the standard steel substrate this is apparent as exsolutions, while in the nitrided samples the Fe oxide layer is located between two cobalt layers. Chromium in both samples created an oxide layer below the Fe containing scale, while manganese is present both in the scale and in the original coating. For the standard steel substrate sample, the iron breakaway took place below the coating. The green cobalt EDS map helps to identify the coating. In the nitrided sample, in contrast, the iron containing oxide was found between two thin cobalt layers, as shown by the light-green element map.

A possible explanation for the corrosion process in ALD-coated samples is a combination of chemical and mechanical iron breakaway. Considering the uniform thickness of Fe distribution in Fig. 6b, the iron experienced uniform migration. In Fig. 6a as well, there is some iron contamination of the coating where the scale is thinner. This can be assumed to be the general corrosion process. The enhanced corrosion regions shown in Fig. 6a instead originate in precise locations, implying a coating failure at those locations. A first delamination and a consequent cracking of the thin protective coating is the suggested explanation. Moreover, the ALD coating might experience oxygen diffusion. The ALD deposited coating behaviour in blocking element diffusion in fact changes completely depending on the chemistry of the substrate and of the deposited chemicals [38]. This aspect is studied for materials used in the semiconductor industry, which is not the case of Mn,Co spinel oxides. A specific investigation, with more sophisticated techniques, would be needed to confirm the oxygen diffusion through the ALD coatings, as

the SEM resolution is not high enough. Another element to consider is that the as-deposited coating could contain fabrication defects.

The constant and generally thin scale formation with all coating compositions ensured a reasonable resistance result, with ASR values contained in the 15–60 mΩ*cm^2 range. The chromium barrier function of the coating was instead only partially fulfilled (Fig. 3), possibly due to the very thin layer allowing for chromium diffusion through the layer.

According to these results and for the chosen temperature conditions, protective coatings for MIC steels deposited with the ALD technique appeared not to be suitable for SOFC application. The 5th batch, MCF coating on nitrided stainless steel, hence did not contain any more samples coated by ALD (Table 1).

A main objective for this study is, as said, to compare coherent results obtained in the same testing conditions. However, it is also interesting to see how the results obtained compare to those present in literature. The wide ranges in the following reported ASR values, prevent a robust benchmarking just considering data present in literature.

Atmospheric plasma spraying is an established solution for SOFC ferritic stainless steel interconnects. APS coated MICs have been assessed in SOFC stacks on the long term [39]. ASR values of metal samples coated with spinel via APS are found to be between 10 and 50 mΩ*cm^2 [40–43]. APS guarantees a dense and thick coating, therefore chromium retention properties are constantly good.

Physical vapour deposition as deposition technique for SOFC MICs is often tested in universities, but, because of the high costs, it is less encountered in real application. The ASR results are mostly good with values below 20 mΩ*cm^2 [15,44,45]. However, there are exceptions. A slightly higher ASR value for MCO spinel coating fabricated with magnetron sputtering is recorded [46] and a deposition of manganese cobalt based spinel via epitaxial beam on Crofer substrates resulted in ASR values above 1 Ω*cm^2 [47].

Articles describing the behaviour of coating deposited with low temperature methods are scarce in literature as the poor density of the coatings leads to modest ASR performances. On the other hand, these methods are actually the most interesting for real SOFC application thanks to their competitive cost. Some examples in literature confirm higher ASR values and un-satisfying Cr retention properties [48,49].

4. Conclusions

More than 60 different combinations of coated metal interconnect materials for the use in SOFC were compared in this study. Specifically, relations and comparisons between steel substrates, substrate pretreatment, coating composition, and coating deposition techniques were observed and evaluated through their Cr retention and contact resistance properties. These results were obtained with small samples tested *ex-situ*, simulating the MIC/cathode interface inside a SOFC stack. The
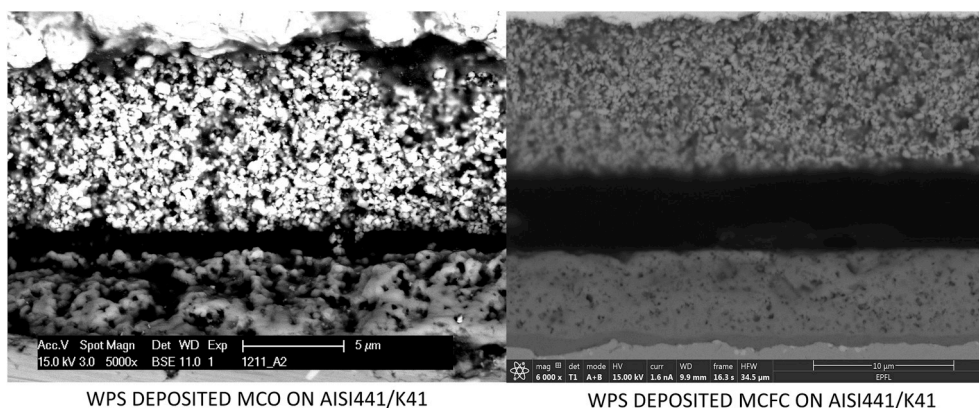

WPS DEPOSITED MCO ON AISI441/K41　　　　　　　　　　　　WPS DEPOSITED MCFC ON AISI441/K41

Fig. 5. On the left, WPS-deposited MCO coating displaying open porosity, on the right WPS-deposited MCFC coating containing closed porosity, after 1000 h at 700 °C in humid (3 vol% H_2O) air.

a) ALD deposited MCO on standard Sandvik Sanergy HT

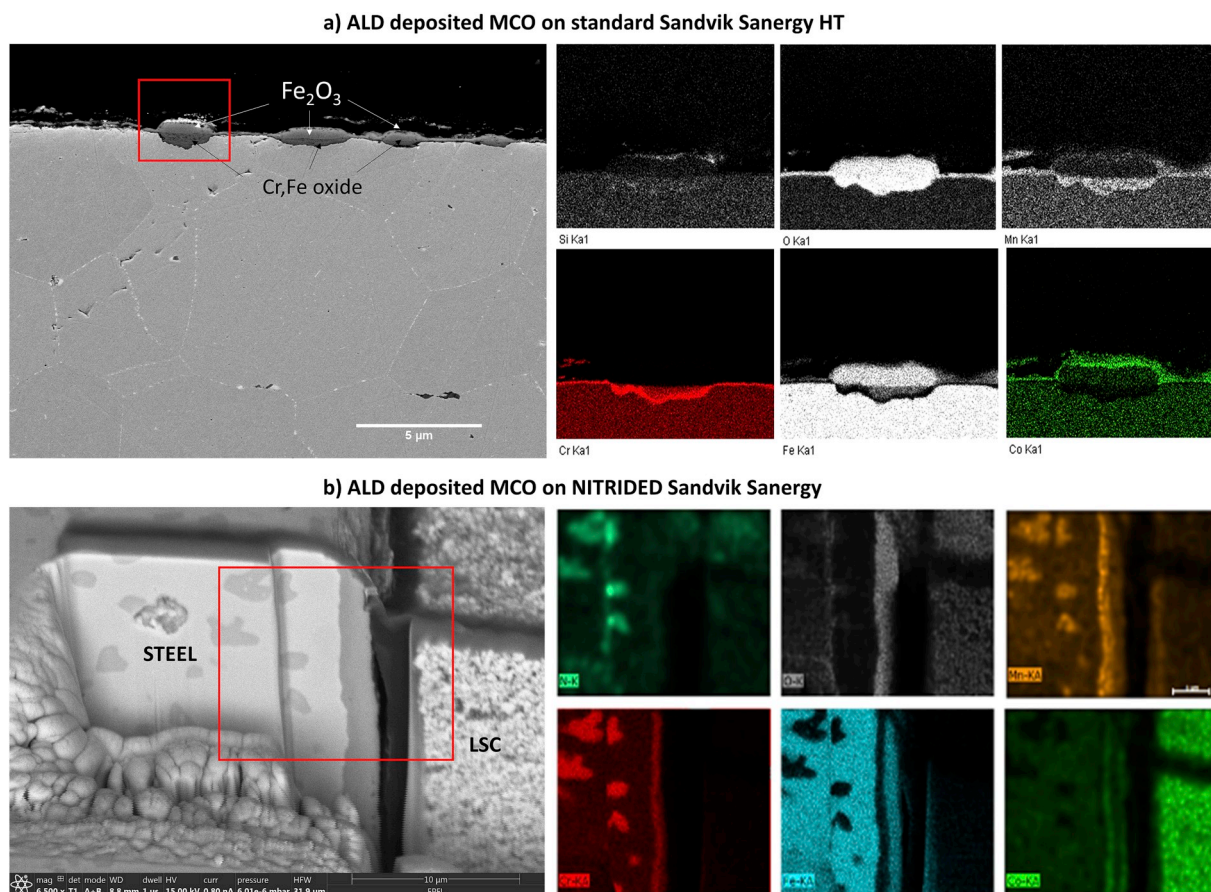**b) ALD deposited MCO on NITRIDED Sandvik Sanergy**

Fig. 6. The top micrograph of an SSHT/MCO interface in batch1 sample with ALD coated MCO shows clearly visible Fe breakaway regions. On the bottom FIB/SEM EDS of similar interface but on a batch2 sample (nitrided steel), also ALD MnCo-coated.

main results offer indications for choices of MIC materials and their coatings. According to the project results it can be summarized that:

- Coating microstructure is key: independently of coating composition and steel substrate type, a (sufficiently thick) dense coating is the most important parameter to ensure a low corrosion rate, high Cr retention, and low contact resistance. Notably, APS- and PVD-deposited coatings were the most effective in limiting MIC degradation.
- The best solution was obtained for Fe-doped MCO-deposited by PVD, with a performance identical to the reference solution SS HT Ce–Co coating, i.e. $\approx 5 m\Omega * cm^2$ at 1000 h of testing.
- Alloying influence: considering ASR and Cr retention results (Figs. 2 and 3), commercial AISI441/K41 (18 wt.% Cr) showed a comparable behaviour to the higher alloyed steels Crofer 22 H and Sandvik Sanergy HT (23 wt.% Cr) when combined with APS or PVD coating. No steel substrates consistently outclassed the others for any coating composition or deposition technique.
- Nitriding of steel substrates is an effective solution to improve Cr retention properties in the case of porous coatings.
- Composition influence: among the tested variations, no coating composition stood out with respect to the others with the exception of Cu-dopied MCF, leading to densification. Hence, the change in coating composition has less influence for the performance than the coating deposition technique.

Acknowledgements

References

[1] M. Bertoldi, O. Bucheli, A. Ravagni, Development, manufacturing and deployment of SOFC-based products at SOLIDpower, ECS Trans 78 (2017) 117–123.
[2] A. Mai, F. Fleischhauer, R. Denzler, J.G. Grolig, M. Dold, A. Schuler, HEXIS galileo 1000 N and HEXIS' next generation SOFC system, in: XIII Eur. SOFC SOEC Forum, Lucerne, n.d.: pp. 5–12.
[3] WORLD ENERGY COUNCIL, World Energy Resources 2016, World Energy Council 2016, 2016. https://www.worldenergy.org/wp-content/uploads/2016/10/World -Energy-Resources-Full-report-2016.10.03.pdf.
[4] J. Wu, X. Liu, Recent development of SOFC metallic interconnect, J. Mater. Sci. Technol. 26 (2010) 293–305, https://doi.org/10.1016/S1005-0302(10)60049-7.
[5] W.Z. Zhu, S.C. Deevi, Development of interconnect materials for solid oxide fuel cells, Mater. Sci. Eng. A 348 (2003) 227–243, https://doi.org/10.1016/S0921-5093(02)00736-0.
[6] J. Piron-Abellan, F. Tietz, V. Shemet, A. Gil, T. Ladwein, L. Singheiser, W. J. Quadakkers, Long term oxidation behaviour and compatibility with contact materials of newly developed ferritic interconnector steel, in: Lucerne, 2002, pp. 248–256.
[7] H. Yokokawa, T. Horita, K. Yamaji, H. Kishimoto, T. Yamamoto, M. Yoshikawa, Y. Mugikura, K. Tomida, Chromium poisoning of LaMnO3-based cathode within generalized approach, Fuel Cells 13 (2013) 526–535, https://doi.org/10.1002/fuce.201200164.
[8] N. Shaigan, W. Qu, D.G. Ivey, W. Chen, A review of recent progress in coatings, surface modifications and alloy developments for solid oxide fuel cell ferritic

stainless steel interconnects, J. Power Sources 195 (2010) 1529–1542, https://doi.org/10.1016/j.jpowsour.2009.09.069.

[9] R. Wang, Z. Sun, U.B. Pal, S. Gopalan, S.N. Basu, Mitigation of chromium poisoning of cathodes in solid oxide fuel cells employing CuMn1.8O4 spinel coating on metallic interconnect, J. Power Sources 376 (2018) 100–110, https://doi.org/10.1016/j.jpowsour.2017.11.069.

[10] M. Bobruk, S. Molin, M. Chen, T. Brylewski, P.V. Hendriksen, Sintering of MnCo2O4 coatings prepared by electrophoretic deposition, Mater. Lett. 213 (2018) 394–398, https://doi.org/10.1016/j.matlet.2017.12.046.

[11] X. Zhang, P.F. You, H.L. Zhang, X.G. Yang, M.Q. Luo, C. Zeng, Preparation and performances of CuCo spinel coating on ferritic stainless steel for solid oxide fuel cell interconnect, Int. J. Hydrogen Energy 43 (2018) 3273–3279, https://doi.org/10.1016/j.ijhydene.2017.12.133.

[12] S.T. Hashemi, A.M. Dayaghi, M. Askari, P.E. Gannon, Sol-gel synthesis of Mn1.5Co1.5O4 spinel nano powders for coating applications, Mater. Res. Bull. 102 (2018) 180–185, https://doi.org/10.1016/j.materresbull.2018.02.040.

[13] Y.T. Yu, J.H. Zhu, Communication—reactive sintering of a CoFe2O4 coating on ferritic stainless steels for SOFC interconnect application, J. Electrochem. Soc. 165 (2018) F297–F299, https://doi.org/10.1149/2.0521805jes.

[14] Y.T. Yu, J.H. Zhu, B.L. Bates, Effect of precursor materials on the performance of the NiFe2O4-based spinel layer for SOFC cathode-side contact application, Solid State Ion. 324 (2018) 40–48, https://doi.org/10.1016/j.ssi.2018.05.030.

[15] H. Falk-Windisch, J. Claquesin, M. Sattari, J.-E. Svensson, J. Froitzheim, Co- and Ce/Co-coated ferritic stainless steel as interconnect material for intermediate temperature solid oxide fuel cells, J. Power Sources 343 (2017) 1–10, https://doi.org/10.1016/j.jpowsour.2017.01.045.

[16] T. Brylewski, A. Kruk, M. Bobruk, A. Adamczyk, J. Partyka, P. Rutkowski, Structure and electrical properties of Cu-doped Mn-Co-O spinel prepared via soft chemistry and its application in intermediate-temperature solid oxide fuel cell interconnects, J. Power Sources 333 (2016) 145–155, https://doi.org/10.1016/j.jpowsour.2016.09.136.

[17] C.-H. Park, K.-H. Baik, Improvements in oxidation resistance and conductivity of Fe-Cr metallic interconnector by (La0.8Ca0.2)(Cr0.9Co0.1)O3 coating, Met. Mater. Int. 20 (2014) 63–67, https://doi.org/10.1007/s12540-014-1005-1.

[18] N.S. Waluyo, R.-H. Song, S.-B. Lee, T.-H. Lim, S.-J. Park, J.-W. Lee, Electrophoretically deposited LaNi0.6Fe0.4O3 perovskite coatings on metallic interconnects for solid oxide fuel cells, J. Electrochem. Soc. 163 (2016) F1245–F1250, https://doi.org/10.1149/2.1171610jes.

[19] K. Przybylski, T. Brylewski, E. Durda, R. Gawel, A. Kruk, Oxidation properties of the Crofer 22 APU steel coated with La0.6Sr0.4Co0.2Fe0.8O3 for IT-SOFC interconnect applications, J. Therm. Anal. Calorim. 116 (2014) 825–834, https://doi.org/10.1007/s10973-013-3594-1.

[20] M. del M. Juez Lorenzo, V. Kolarik, V. Kuchenreuther-Hummel, M. Pötschke, D. Schimanke, Oxidation of La–Sr–Mn-coated interconnector alloys for steam electrolysis under pressure in pure oxygen and in pure steam, Oxid. Metals 88 (2017) 279–290, https://doi.org/10.1007/s11085-017-9736-2.

[21] S. Frangini, A. Masi, L.D. Seta, M. Bianco, J.V. Herle, Composite Cu-LaFeO3 conversion coatings on a 18Cr ferritic stainless steel for IT-SOFC application: effect of long-term air exposure at 700°C on Cr diffusion barrier and electrical properties, J. Electrochem. Soc. 165 (2018) F97–F104, https://doi.org/10.1149/2.0101803jes.

[22] M. Stygar, W. Tejchman, J. Dąbrowa, A. Kruk, T. Brylewski, Synthesis, processing and properties of calcium- and nickel-doped yttrium chromates(III) Y0.8Ca0.2Cr1−xNixO3 (x = 0-0.3) and studies on their potential application as coatings for SOFC interconnects, J. Mater. Eng. Perform. 27 (2018) 3276–3289, https://doi.org/10.1007/s11665-018-3422-7.

[23] F. Saeidpour, M. Zandrahimi, H. Ebrahimifar, Evaluation of pulse electroplated cobalt/yttrium oxide composite coating on the Crofer 22 APU stainless steel interconnect, Int. J. Hydrogen Energy 44 (2019) 3157–3169, https://doi.org/10.1016/j.ijhydene.2018.12.062.

[24] S. Molin, P. Jasinski, L. Mikkelsen, W. Zhang, M. Chen, P.V. Hendriksen, Low temperature processed MnCo2O4 and MnCo1.8Fe0.2O4 as effective protective coatings for solid oxide fuel cell interconnects at 750 °C, J. Power Sources 336 (2016) 408–418, https://doi.org/10.1016/j.jpowsour.2016.11.011.

[25] M.W. Lundberg, R. Berger, J. Westlinder, Multilayered PVD coating for interconnector steel, in: Proc. XI Eur. SOFC SOE Forum 2014, 2014, pp. 5–11. Lucerne.

[26] K41 technical data sheet, ArcelorMittal, n.d. http://www.aperam.com/uploads/stainlesseurope/TechnicalDataSheet/FT_K41X_Eng.pdf (accessed November 15, 2017).

[27] J. Tallgren, M. Bianco, J. Mikkola, O. Himanen, M. Rautanen, J. Kiviaho, J. Van herle, Comparison of different manganese-cobalt-iron spinel protective coating for SOFC interconnects, in: XII European SOFC & SOE Forum, 2016, pp. 114–124.

[28] J. Tallgren, M. Bianco, O. Himanen, O. Thomann, J. Kiviaho, J. van Herle, Evaluation of protective coatings for SOFC interconnects, ECS Trans 68 (2015) 1597–1608, https://doi.org/10.1149/06801.1597ecst.

[29] J. Froitzheim, G.H. Meier, L. Niewolak, P.J. Ennis, H. Hattendorf, L. Singheiser, W. J. Quadakkers, Development of high strength ferritic steel for interconnect

application in SOFCs, J. Power Sources 178 (2008) 163–173, https://doi.org/10.1016/j.jpowsour.2007.12.028.

[30] E.A. Polman, T. Fransen, P.J. Gellings, The reactive element effect; ionic processes of grain-boundary segregation and diffusion in chromium oxide scales, J. Phys. Condens. Matter 1 (1989) 4497, https://doi.org/10.1088/0953-8984/1/28/001.

[31] R. Scataglini, M. Wei, A. Mayyas, S.H. Chan, T. Lipman, M. Santarelli, A direct manufacturing cost model for solid-oxide fuel cell stacks, Fuel Cells 17 (2017) 825–842, https://doi.org/10.1002/fuce.201700012.

[32] Manufacturing Cost Analysis of 1 kW and 5 kW Solid Oxide Fuel Cell (SOFC) for Auxilliary Power Applications, BATTELLE, Battelle Memorial Institute 505 King Avenue Columbus, OH 43201, 2014, pp. 43–47. https://energy.gov/sites/prod/files/2014/06/f16/fcto_battelle_cost_analysis_apu_feb2014.pdf. (Accessed 10 February 2017).

[33] A. Holt, P. Kofstad, Electrical conductivity of Cr2O3 doped with TiO2, Solid State Ion. 117 (1999) 21–25, https://doi.org/10.1016/S0167-2738(98)00244-6.

[34] M.P. Brady, K. Weisbrod, C. Zawodzinski, I. Paulauskas, R.A. Buchanan, L. R. Walker, Assessment of thermal nitridation to protect metal bipolar plates in polymer electrolyte membrane fuel cells, Electrochem. Solid State Lett. 5 (2002) A245–A247, https://doi.org/10.1149/1.1509561.

[35] Y. Larring, T. Norby, Spinel and perovskite functional layers between plansee metallic interconnect (Cr-5 wt % Fe-1 wt % Y 2 O 3) and ceramic (La0.85Sr0.15) 0.91MnO3 cathode materials for solid oxide fuel cells, J. Electrochem. Soc. 147 (2000) 3251–3256, https://doi.org/10.1149/1.1393891.

[36] R. Steinberger-Wilckens, S. Yang, K. Cooke, J. Tallgren, O. Himanen, S. Frangini, A. Masi, M. Bianco, J. Van herle, J.-E. Hong, M. Oum, F. Bozza, A. Dellai, Benchmarking Protective Coatings for SOFC Ferritic Steel Interconnects – the SCORED 2:0 Project, 2016, pp. 41–50.

[37] L. Blum, L.G.J. (Bert) de Haart, J. Malzbender, N.H. Menzler, J. Remmel, R. Steinberger-Wilckens, Recent results in Jülich solid oxide fuel cell technology development, J. Power Sources 241 (2013) 477–485, https://doi.org/10.1016/j.jpowsour.2013.04.110.

[38] M. Knez, Diffusion phenomena in atomic layer deposition, Semicond. Sci. Technol. 27 (2012), 074001, https://doi.org/10.1088/0268-1242/27/7/074001.

[39] S.M. Groß-Barsnick, Q. Fang, P. Batfalsky, L. Niewolak, L. Blum, W.J. Quadakkers, Post-test characterization of metallic materials and adjacent components in an SOFC stack after 34,000 h operation at 700 °C, Fuel Cells 19 (2019) 84–95, https://doi.org/10.1002/fuce.201800050.

[40] Y.-Z. Hu, S.-W. Yao, C.-X. Li, C.-J. Li, S.-L. Zhang, Influence of pre-reduction on microstructure homogeneity and electrical properties of APS Mn1.5Co1.5O4 coatings for SOFC interconnects, Int. J. Hydrogen Energy 42 (2017) 27241–27253, https://doi.org/10.1016/j.ijhydene.2017.09.073.

[41] R. Spotorno, P. Piccardo, F. Perrozzi, S. Valente, M. Viviani, A. Ansar, Microstructural and electrical characterization of plasma sprayed Cu-Mn oxide spinels as coating on metallic interconnects for stacking solid oxide fuel cells, Fuel Cells 15 (2015) 728–734, https://doi.org/10.1002/fuce.201400189.

[42] J. Puranen, M. Pihlatie, J. Lagerbom, T. Salminen, J. Laakso, L. Hyvärinen, M. Kylmälahti, O. Himanen, J. Kiviaho, P. Vuoristo, Influence of powder composition and manufacturing method on electrical and chromium barrier properties of atmospheric plasma sprayed spinel coatings prepared from MnCo2O4 and Mn2CoO4 + Co powders on Crofer 22 APU interconnectors, Int. J. Hydrogen Energy 39 (2014) 17246–17257, https://doi.org/10.1016/j.ijhydene.2014.08.016.

[43] M.J.G. Vargas, M. Zahid, F. Tietz, A. Aslanides, Use of SOFC metallic interconnect coated with spinel protective layers using the APS technology, ECS Trans 7 (2007) 2399–2405, https://doi.org/10.1149/1.2729362.

[44] V.I. Gorokhovsky, P.E. Gannon, M.C. Deibert, R.J. Smith, A. Kayani, M. Kopczyk, D. VanVorous, Z. Yang, J.W. Stevenson, S. Visco, C. Jacobson, H. Kurokawa, S. W. Sofie, Deposition and evaluation of protective PVD coatings on ferritic stainless steel SOFC interconnects, J. Electrochem. Soc. 153 (2006) A1886–A1893, https://doi.org/10.1149/1.2266244.

[45] K.O. Hoyt, P.E. Gannon, P. White, R. Tortop, B.J. Ellingwood, H. Khoshuei, Oxidation behavior of (Co,Mn)3O4 coatings on preoxidized stainless steel for solid oxide fuel cell interconnects, Int. J. Hydrogen Energy 37 (2012) 518–529, https://doi.org/10.1016/j.ijhydene.2011.09.028.

[46] Q. Fu, F. Tietz, D. Sebold, E. Wessel, H.-P. Buchkremer, Magnetron-sputtered cobalt-based protective coatings on ferritic steels for solid oxide fuel cell interconnect applications, Corros. Sci. 54 (2012) 68–76, https://doi.org/10.1016/j.corsci.2011.08.051.

[47] V. Miguel-Pérez, A. Martínez-Amesti, M.L. Nó, J. Calvo-Angós, M.I. Arriortua, EB-PVD deposition of spinel coatings on metallic materials and silicon wafers, Int. J. Hydrogen Energy 39 (2014) 15735–15745, https://doi.org/10.1016/j.ijhydene.2014.07.115.

[48] S.R. Akanda, N.J. Kidner, M.E. Walter, Spinel coatings on metallic interconnects: effect of reduction heat treatment on performance, Surf. Coat. Technol. 253 (2014) 255–260, https://doi.org/10.1016/j.surfcoat.2014.05.049.

[49] N. Hosseini, M.H. Abbasi, F. Karimzadeh, G.M. Choi, Development of Cu1.3Mn1.7O4 spinel coating on ferritic stainless steel for solid oxide fuel cell interconnects, J. Power Sources 273 (2015) 1073–1083, https://doi.org/10.1016/j.jpowsour.2014.10.017.